Theoretical and Experimental (Electron-Impact) Studies of the Low-Lying Rydberg States in O_2†

David C. Cartwright
Chemistry and Physics Laboratory, The Aerospace Corporation, El Segundo, California 90045

W. J. Hunt*
Arthur A. Noyes Laboratory for Chemical Physics, California Institute of Technology, Pasadena, California 91109

W. Williams and S. Trajmar
California Institute of Technology, Jet Propulsion Laboratory, Pasadena, California 91103

W. A. Goddard, III‡
Arthur A. Noyes Laboratory for Chemical Physics, California Institute of Technology, Pasadena, California 91109
(Received 14 May 1973)

Theoretical studies of the $n = 3$, 4, and 5 Rydberg series in O_2, converging to $O_2^+(X\ ^2\Pi_g)$, are presented and correlated with electron energy-loss spectra of molecular oxygen, in the region from 7.0 to 10.5 eV. The energy-loss spectra have been studied as a function of the scattering angle for a incident electron energy of 45 eV. The angular dependence determined for various features in the energy-loss spectra have been correlated with the known behavior for transitions between electronic states of certain symmetry, and with the theoretical results, to identify the low-lying Rydberg states. Four vibrational levels of the $(3s\,\sigma_g)\ ^3\Pi_g$ Rydberg state have been observed superposed on top of the maximum intensity portion of the Schumann-Runge continuum with $T_{00} = 8.145 \pm 0.020$ eV. The theoretical results, combined with the energy-loss measurements and the high-resolution photon-absorption work, lead to the assignment of the lowest dipole-allowed $^3\Sigma_u^-$ and $^3\Pi_u$ Rydberg states at $T_{00} \leq 9.31$ eV and $T_{00} = 9.97$ eV, respectively.

I. INTRODUCTION

Considerable work has been done on the photoabsorption spectrum of molecular oxygen in the 6–12.5-eV region,[1] but relatively few of the Rydberg states in that region have been identified, primarily owing to the diffuseness of the observed bands. In the case of O_2, information about the Rydberg states can also be obtained by photon absorption measurements in which the initial state is one of the two low-lying metastable electronic states.[1-5] Because of the fairly restrictive selection rules which determine the strength of a transition in photoabsorption, only a relatively small fraction of the total number of Rydberg states can be readily studied by either of these photoabsorption techniques. Many more excited electronic states can be studied through the use of electron-impact spectroscopy, although the spectral resolution is usually poorer than in photoabsorption work. In cases where the observed bands are broadened by perturbations, as is the case for many bands in O_2, a study of the angular distributions determined from electron-impact spectroscopy can provide useful information[6] as to the location and symmetry of excited electronic states which is otherwise not attainable. The results of some electron-impact work on O_2 have been reported by Lassettre and co-workers[7] for electron-impact energies of 48 eV and greater, and for scattering angles less than 15°. Geiger and Schroeder[8] have studied the electron absorption spectrum for high impact energy (25 keV) and forward scattering ($\theta \approx 0°$) and obtained some new information concerning progressions of Rydberg states above 16 eV. Trajmar *et al.*[9] have recently studied the electron energy-loss spectrum in O_2 for various electron energies from 4 to 45 eV and scattering angles out to 90°. This work resulted in normalized integral cross sections for excitation of various electronic states of O_2,[9(a)] the angular dependence of the electron-impact excitation for many of the valence excited states of O_2,[9(b)] and a rigorous selection rule for electron-impact excitation of diatomic molecules.[10] A new technique employing an electron transmission spectrometer, which has been used to study[11] the core-excited resonances of O_2, also provides some information about the excited states of the neutral molecule.

In this paper,[12] the electron-impact energy-loss spectra of O_2 in the region 7–10.5 eV are examined in an effort to locate and characterize the low-lying Rydberg states. The results from the energy-loss spectra are combined with *ab initio* calculations reported here and correlated with the available high-resolution work to locate the lowest two Rydberg states that are dipole con-

nected to the ground electronic state, and the first member of the $(ns\sigma_g)\,^3\Pi_g$ Rydberg series. Normalized angular distributions for the excitation of these states by 45-eV incident electrons are also obtained.

II. EXPERIMENTAL

The basic electron-impact spectrometer used to collect the data reported here has been discussed in detail in earlier publications.[13] An energy-selected electron beam is scattered off a gaseous O_2 target at a pressure of the order of 1 mTorr. The scattered electron intensity, as a function of energy loss, is measured at a fixed impact energy E_0 and scattering angle θ. The scattering angle can be changed from $-30°$ to $+90°$, and the true zero angle is determined by the symmetry of the scattered intensity for an inelastic feature near the nominal zero angle. The impact energy scale was calibrated by mixing He and O_2 and locating the 19.3-eV He resonance.

Examples of the energy-loss spectra are shown in Fig. 1 for an incident energy of 45 eV and scattering angles of 15° and 25°. These spectra are the result of repetitive scans using a 1024-channel analyzer requiring several hours at each scattering angle to achieve the desired signal-to-noise ratio. The "longest band" at 9.97 eV[14] and the "second band" at 10.29 eV,[15] as well as the broad Schumann-Runge continuum from 6.9 to about 9.4 eV, dominate the energy-loss spectra at these scattering angles. Of primary interest in this paper are the Rydberg states which fall in this energy-loss region. In addition to the longest and second bands, the vibrational structure appearing on top of the Schumann–Runge continuum and small peaks on the low-energy-loss side of the longest band are readily discernible in Fig. 1. Before analyzing the experimental results, an account of the theoretical predictions of the Rydberg structure in this energy-loss region is given.

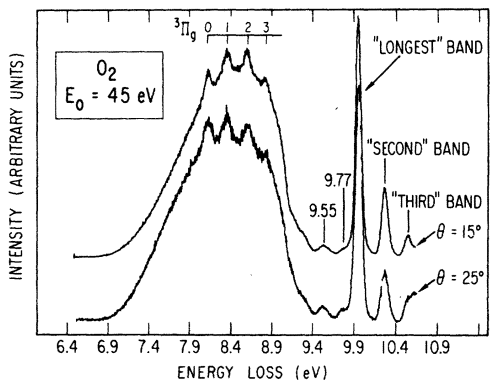

FIG. 1. Electron energy-loss spectra in molecular oxygen for an incident electron energy of 45 eV and scattering angles of 15° and 25°. The vibrational structure on top of the Schumann–Runge continuum is assigned to the $(3s\sigma_g)\ ^3\Pi_g$ Rydberg state, and the features at 9.31, 9.55, and 9.77 eV are assigned to the $(3p\pi_u)\ ^3\Sigma_u^-$ Rydberg state. The strong feature at 9.97 eV ("longest" band) is assigned to the $(3p\sigma_u)\ ^3\Pi_u$ Rydberg state.

III. THEORY

A. Improved Virtual-Orbital Method

In the Hartree–Fock method, the occupied orbitals are obtained by solving for eigenfunctions of an appropriate one-particle effective Hamiltonian which is derived from a variational principle. The unoccupied eigenfunctions of this Hamiltonian are called virtual orbitals and are often used to obtain approximate excited state wave functions. However, such virtual orbitals are very poor approximations for the excited states because the effective Hamiltonian, of which they are eigenfunctions, corresponds to an N-electron core rather than an $(N-1)$-electron core. The alternative of solving self-consistently for each excited electronic state is quite time consuming when the entire spectrum of excited states is of interest. In addition, general open-shell techniques have only recently been developed[16] and programmed to actually carry out calculations on the types of complicated open shells occurring in many of the excited states of O_2.

An intermediate approach has recently been developed and used by Hunt and Goddard[17] in which the form of the Hartree–Fock Hamiltonian is modified so that the virtual orbitals are good approximations to the self-consistent excited-state orbitals. These orbitals are called *improved virtual orbitals* (IVO) and form variationally optimum excited-state orbitals within the restriction that the other $N-1$ electrons are in ground-state orbitals. An approach leading to equivalent wave functions has also been suggested and used by Lefebvre-Brion and Moser,[18] wherein they carried out configuration-interaction (CI) calculations using single excitations from appropriate orbitals.

The eigenvalue of the IVO, ϵ_R, corresponds to its ionization potential (the ionic limit with orbital ϕ_R removed) and is generally accurate to 0.2 eV for Rydberg states. This accuracy can be achieved because the correlation error for the excited state is primarily due to the $N-1$ electron core and this core is essentially unchanged upon ionization (from the excited orbital). In order to obtain the excitation energy from the ground state to this particular state, say $\phi_i \rightarrow \phi_R$, the ionization potential ϵ_i to remove orbital ϕ_i from the

ground state is also needed. However, Hartree–Fock calculations generally yield relatively poor values for ionization potentials from the ground state (≈1-eV errors) owing to the large correlation errors for cases with doubly occupied orbitals. For this reason the excitation energies ΔE reported here were obtained by using the calculated ϵ_R but the experimental value of ϵ_i (note that $\epsilon < 0$):

$$\Delta E(i \rightarrow R) = \epsilon_R(\text{calc}) - \epsilon_i(\text{exper}). \quad (1)$$

The zero-point energy is expected to be the same in the Rydberg state as in the ion so that if the adiabatic ionization potential is used in (1), the resulting ΔE corresponds to the T_{00} value for the Rydberg state. In addition, since the potential curve for the Rydberg state is expected to be parallel to that for the (corresponding) ion state (but lower in energy by ϵ_R), a single calculation (say at R_e) for the ground state generally results in reliable diabatic potential-energy curves for the Rydberg states.

It is noted that the IVO procedure is not expected to be as useful for excited states whose excited orbital is valencelike (having the size of $n=2$ orbitals for O_2). The reason is that, in this case, it is no longer possible to assume that the correlation energy is the same in the excited state and the ion formed with the $N-1$ electron core. Indeed, in many cases, it is better to assume that the correlation error is comparable in the ground and valence excited states. In addition, rearrangements of the orbitals for the other $N-1$ electrons can have an important effect on a valence excited orbital. In the case of Rydberg states, these difficulties are not encountered and the IVO method provides a good description of these excited states.

B. Calculational Details

For the calculation of the ground state, the $4s3p$ contracted Gaussian basis set described by Dunning[19] (26 contracted basis functions obtained from 48 primitive Gaussians) was used. In order to obtain a good description of $(n=3)$- and $(n=4)$-type Rydberg states a set $[4s\ 3p\ 2d]$ of low-exponent (diffuse) Gaussian functions[20] was added to the above basis. Large-exponent (valencelike) d functions were not used since other calculations[17,20] have indicated that they have a negligible effect on the position of the Rydberg states.

The method of forming the IVO Hamiltonians is straightforward and outlined elsewhere.[17,20] The calculations were carried out with the Caltech SCF/GVB wave-function programs[16,21] and the Polyatom integral programs.[22]

C. Excited States

In the simple-molecular-orbital (MO) model, the wave function of the ground state of O_2 has the configuration

$$(1\sigma_g)^2(1\sigma_u)^2(2\sigma_g)^2(2\sigma_u)^2(3\sigma_g)^2(1\pi_u)^4(1\pi_g)^2$$

leading to $^3\Sigma_g^-$, $^1\Delta_g$, and $^1\Sigma_g^+$ states. The lowest ionization limit corresponds to removing the $1\pi_g$ orbital, leaving the core in the $X^2\Pi_g$ state. Below this ionization limit there are two basic types of excited states: (a) valence states formed from transitions such as $1\pi_u \rightarrow 1\pi_g$ or $3\sigma_g \rightarrow 1\pi_g$, which are excitations from occupied orbitals into the partially filled $1\pi_g$ orbital; and (b) Rydberg states formed by transitions from the $1\pi_g$ valence orbital into $3s$, $3p$, $4s$, $4p$, $3d$, etc., Rydberg orbitals. These Rydberg orbitals are much larger spatially than the valence orbitals and correspond approximately to an atomic orbital with principal quantum number ≥ 3. The states formed by excitation from the $1\pi_g$ orbital to the valencelike $3\sigma_u$ antibonding orbital can be characterized as valence states (a) although the $3\sigma_u$ orbital possesses a moderate amount of diffuse character.

The T_{00} values calculated for the Rydberg states formed by excitation from a $1\pi_g$ MO are summarized in Table I. The final-state orbital is given in column 1. Columns 2 and 3, and 4 and 5, are the symmetries and excitation energies, for the triplet and singlet states, respectively. Columns 6 and 7 are, respectively, the *average* excitation energy and ionization potential for each Rydberg orbital. These values were obtained by averaging the results obtained for the singlet and triplet states formed from the Rydberg orbital. These average values show how the excitation energies approximately group according to the n and l quantum numbers of the Rydberg orbital.

The lowest $^3\Pi_g$ and $^1\Pi_g$ Rydberg states, corresponding to the orbital transition $1\pi_g \rightarrow 3s\sigma_g$, are calculated to lie 8.23 and 8.34 eV, respectively, above the ground electronic state. The $^3\Pi_g$ state is observed in the electron energy-loss spectra (see Sec. IV) with $T_{00} = 8.145 \pm 0.020$ eV but the $^1\Pi_g$ state was not detected (it might overlap higher vibrational levels of the observed $^3\Pi_g$).

Excitation from the $1\pi_g$ orbital to a $3p\pi_u$ Rydberg orbital results in the six Rydberg states (calculated T_{00} values in parentheses): $^1\Sigma_u^-$ (9.26), $^3\Delta_u$ (9.34), $^3\Sigma_u^+$ (9.41), $^3\Sigma_u^-$ (9.44), $^1\Delta_u$ (9.54), and $^1\Sigma_u^+$ (9.63). The ordering of these states can be understood by considering just the electron repulsion energy between the $1\pi_g$ and $3p\pi_u$ singly occupied orbitals. That is, expanding the two-electron spatial part of the wave function, e.g., for the $^1\Sigma_u^-$, one obtains $(\pi_g^+\pi_u^- - \pi_g^-\pi_u^+ + \pi_u^-\pi_g^+$

$-\pi_u^+\pi_g^-$). If the same orbitals are used for each of the states, the relative energies of these states can be expressed in terms of the J_0, K_0, J_2, K_2 electron-repulsion integrals, as in Table II. Since these integrals should be in the order

$$J_0 > K_0 > J_2 > K_2 ,$$

the electronic states are ordered as in Table II, which agrees with the ordering of the IVO states (see Table I). Of these six Rydberg states, only $^3\Sigma_u^-$ is dipole connected to the ground electronic state. As discussed in Sec. IV, the calculations and experiments reported herein have resulted in the assignment of this state in electron energy-loss spectra. The $^1\Delta_u$ state is dipole connected to the $^1\Delta_g$ state and transitions between these states have been studied by Yamawaki and Ogawa,[5] who obtain $T_{00} = 9.32$ to 9.35 eV.

Excitation from the $1\pi_g$ MO to the $3p\sigma_u$ Rydberg orbital results in $^{3,1}\Pi_u$ electronic states. States of this same symmetry can also be formed by excitation from the $1\pi_g$ to the $3\sigma_u$ valencelike antibonding MO. Calculations using the IVO model place those states formed from the $3\sigma_u$ MO about 2 eV lower than those formed from the $4\sigma_u$ ($=3p\sigma_u$) Rydberg orbital. The assumption in the IVO model that the correlation error in the excited state is the same as in the ion state is not as valid for valence states and should lead to too small an excitation energy for the $3\sigma_u$ valence states. The IVO calculations on these states, included in Table I for completeness, place the $^3\Pi_u(V)$ state at 7.99 eV, whereas it is most likely located about 8.5 eV above the ground state at the R_e of the latter.

Since the $^3\Pi_u$ valence and Rydberg states differ by the single-orbital excitation [$3\sigma_u \rightarrow 4\sigma_u$ ($3p\sigma_u$)], the $4\sigma_u$ orbital of the $^3\Pi_u(R)$ state must be orthogonal to the $3\sigma_u$ orbital of the valence state. This orthogonality effect is expected to force the $^3\Pi_u(R)$ state to a higher energy than expected for a "normal" $3p$ Rydberg orbital. This is indeed the case as the IVO calculations place the $^3\Pi_u(R)$ state at 9.98 eV, which is 0.59 eV higher than the average of the energies for the other seven states formed from the $3p$ Rydberg orbital. As will be discussed in more detail below, the "longest band" at 9.97 eV is thus identified as the $(3p\sigma_u)$ $^3\Pi_u$ Rydberg state. It is further noted that the equilibrium internuclear distance R_e for the state at 9.97 eV appears to be close to that for the ground state ($R_e = 1.21$ Å), which is about 0.09 Å larger than that for the ion state to which it is converging ($R_e = 1.12$ Å). This can also be explained in terms of the interaction between the Rydberg and valence $^3\Pi_u$ states mentioned above. That is, this interaction should be greater at smaller internuclear distances (because of greater overlap between the $3\sigma_u$ and $4\sigma_u$ orbitals) and

TABLE I. Theoretical T_{00} values (eV) for Rydberg states of O_2. The excitation energies were obtained by using an IP($1\pi_g$) = 12.07 eV (Ref. 27). All cases are $1\pi_g \rightarrow \phi_R$.

Orbital	Triplet states (eV)		Singlet states (eV)		Average[a] ΔE(eV)	IP(eV)
$3\sigma_u$	$^3\Pi_u$	7.99[b]	$^1\Pi_u$	10.46[b]		
$3s\sigma_g$	$^3\Pi_g$	8.23	$^1\Pi_g$	8.34	8.27	3.79
$3p\sigma_u$	$^3\Pi_u$	9.98	$^1\Pi_u$	9.10	9.54	2.53
$3p\pi_u$	$^3\Sigma_u^+$	9.41	$^1\Sigma_u^+$	9.63	9.43	2.63
	$^3\Delta_u$	9.34	$^1\Delta_u$	9.54		
	$^3\Sigma_u^-$	9.44	$^1\Sigma_u^-$	9.26		
$3d\sigma_g$	$^3\Pi_g$	10.39	$^1\Pi_g$	10.41	10.39	1.67
$3d\pi_g$	$^3\Sigma_g^+$	10.60	$^1\Sigma_g^+$	10.64	10.59	1.47
	$^3\Delta_g$	10.58	$^1\Delta_g$	10.62		
	$^3\Sigma_g^-$	10.60	$^1\Sigma_g^-$	10.57		
$4s\sigma_g$	$^3\Pi_g$	10.61	$^1\Pi_g$	10.62	10.60	1.46
$4p\sigma_u$	$^3\Pi_u$	10.96	$^1\Pi_u$	11.10	11.02	1.04
$4p\pi_u$	$^3\Sigma_u^+$	10.86	$^1\Sigma_u^+$	10.93	10.86	1.20
	$^3\Delta_u$	10.84	$^1\Delta_u$	10.91		
	$^3\Sigma_u^-$	10.85	$^1\Sigma_u^-$	10.82		
$4d\sigma_g$	$^3\Pi_g$	11.17	$^1\Pi_g$	11.18	11.16	0.90
$4d\pi_g$	$^3\Sigma_g^+$	11.24	$^1\Sigma_g^+$	11.26	11.23	0.83
	$^3\Delta_g$	11.23	$^1\Delta_g$	11.25		
	$^3\Sigma_g^-$	11.24	$^1\Sigma_g^-$	11.23		
$5s\sigma_g$	$^3\Pi_g$	11.27	$^1\Pi_g$	11.27	11.26	0.80
$5p\sigma_u$	$^3\Pi_u$	11.32	$^1\Pi_u$	11.32	11.31	0.75
$5p\pi_u$	$^3\Sigma_u^+$	11.33	$^1\Sigma_u^+$	11.33	11.31	0.75
	$^3\Delta_u$	11.32	$^1\Delta_u$	11.33		
	$^3\Sigma_u^-$	11.32	$^1\Sigma_u^-$	11.32		

[a] The average of the results for the singlet and triplet states.

[b] For the reasons given in Sec. III A, the IVO results for this valence state are less accurate than those for the Rydberg states.

TABLE II. Energy expressions for the $(1\pi_g)(3p\pi_u)$ states.

	Electron repulsion terms[a] J_0	K_0	J_2	K_2	E(IVO) (eV)
$^1\Sigma_u^+$	1	1	1	1	9.63
$^1\Delta_u$	1	1	0	0	9.54
$^3\Sigma_u^-$	1	1	−1	−1	9.44
$^3\Sigma_u^+$	1	−1	1	−1	9.41
$^3\Delta_u$	1	−1	0	0	9.34
$^1\Sigma_u^-$	1	−1	−1	+1	9.26

[a] Letting

$$(\phi_a\phi_b|\phi_c\phi_d) = \iint d^3x_1\, d^3x_2\, \frac{1}{r_{12}}\, \phi_a(1)\phi_b(1)\phi_c(2)\phi_d(2) ,$$

$$J_0 = (\pi_g^{+1}\pi_g^{-1}|\pi_u^{+1}\pi_u^{-1}) ,$$

$$J_2 = (\pi_g^{+1}\pi_g^{+1}|\pi_u^{-1}\pi_u^{-1}) ,$$

$$K_0 = (\pi_g^{+1}\pi_u^{-1}|\pi_g^{+1}\pi_u^{-1}) ,$$

$$K_2 = (\pi_g^{+1}\pi_u^{+1}|\pi_g^{-1}\pi_u^{-1}) .$$

therefore force the Rydberg state to larger internuclear distances than for a normal $3p$ Rydberg state.

The $^1\Pi_u$ states appear to be similarly affected by Rydberg-valence interactions. If no diffuse functions are allowed in the description of the $^3\Pi_u(V)$ state, the $1\pi_g$, $3\sigma_u$ exchange integral is found to be

$$K_{1\pi_g,3\sigma_u} \cong 1.02 \text{ eV}.$$

The $(3\sigma_u)\ ^1\Pi_u(V)$ state would therefore be expected to be about 2 eV higher than the $^3\Pi_u(V)$ state, or about 10.5 eV above the ground state. By analogous arguments, the $(3p\sigma_u)\ ^1\Pi_u(R)$ state would be expected at about 9.5 eV, so the lowest $^1\Pi_u$ state might be expected to be mainly Rydberg in character. However, there is again expected to be a strong interaction between the Rydberg and valence $^1\Pi_u$ states and the lowest state is expected to have some valence character. As in the case of the $^3\Pi_u$ states, the IVO assumption that the correlation energy is the same in the Rydberg state and ion state to which it converges is not very good for a state with significant valence character and hence results in too low an excitation energy for the $(3p\sigma_u)\ ^1\Pi_u$ state. That is, the $^1\Pi_u(R)$ state is calculated to be at 9.10 eV, which is 0.40 eV below the experimental location based on the work of Yamawaki and Ogawa.[5]

D. *LS*-Versus-*JJ* Coupling

Yamawaki and Ogawa[5] have concluded from photoabsorption studies that JJ coupling is more appropriate than LS coupling for describing the $^{3,1}\Delta_u$ $(np\pi_u)$ Rydberg states. They found two pairs of $^1\Delta_u - {}^1\Delta_g$ transitions, separated by about 201 cm^{-1} [=0.0249 eV, the spin-orbit splitting in the $O_2^+(X^2\Pi_g)$ state] at energies corresponding to the $1\pi_g \rightarrow np\pi_u$ ($n=4$, 5) transitions. However, they did not find strong evidence for doubling in transitions to the $n=3$ Rydberg state. Using LS coupling, the $^3\Delta_u - {}^1\Delta_u$ separations are calculated (Table I) to be 0.20, 0.07, and 0.01 eV for $n=3$, 4, and 5, respectively. Since the separation for the $n=5$ states is smaller than the spin-orbit splitting, these states are better described by JJ coupling and should result in apparent $^1\Delta_u \leftarrow {}^1\Delta_g$ transitions separated by 201 cm^{-1}. Using the calculated $^3\Delta_u - {}^1\Delta_u$ splitting for the $n=4$ states (0.07 eV), and including the spin-orbit splitting observed for the O_2^+ limit (0.025 eV), results in JJ-coupled ($^3\Delta_u$, $^1\Delta_u$) states separated by about 0.08 eV. Based on the appropriate energy differences, the $^3\Delta_u$ state has a 15% singlet character, and vice-versa. For the $n=3$ states, the mixing of the other spin component should be less than 5%. The calculations reported here indicate that the appropriate coupling is LS coupling for the $n=3$ states, JJ coupling for the $n=5$ states, and perhaps intermediate coupling for $n=4$. This is in reasonable agreement with the experimental findings of Yamawaki and Ogawa.[5]

E. Comparison with Other Calculations

There have been very few other calculations reported for the excited states of O_2. LeClercq[23] used the single-excitation (CI) approach of Lefebvre-Brion and Moser,[18] which leads to wave functions which are equivalent to the IVO results. However, the set of expansion functions (the basis) used in their calculations was a minimum basis consisting of one Slater orbital for each atomic orbital plus one additional Slater function on each center for each of the $n=3$ and 4, s and p, Rydberg orbitals. This basis is less than half the size of that used in the calculations reported here (and also does not contain diffuse d-basis functions) and may not be sufficiently flexible to describe the excited states properly. As a result, they found that the $^3\Pi_u$ $(3p\sigma_u)$ state had about

TABLE III. Comparison of theoretical and experimental $1\pi_g \rightarrow \phi_R$ excitation energies.

State		Theoretical ΔE(eV) This work	Experimental ΔE(eV) Lindholm	Ogawa	This work
$3s\sigma_g$	$^3\Pi_g$	8.23			8.145 ± 0.02
	$^1\Pi_g$	8.34			
$3p\sigma_u$	$^3\Pi_u$	9.98	9.77[a]		9.97
	$^1\Pi_u$	9.10[b]		9.50	
$3p\pi_u$	$^1\Sigma_u^-$	9.26			
	$^3\Delta_u$	9.34			
	$^3\Sigma_u^+$	9.41	9.59[a]		
	$^3\Sigma_u^-$	9.44	9.32		≤9.31
	$^1\Delta_u$	9.54	9.34	9.32–9.35	
	$^1\Sigma_u^+$	9.63	9.45		
$3d\sigma_g$	$^3\Pi_g$	10.39			
	$^1\Pi_g$	10.41			
$3d\pi_g$	$^1\Sigma_g^-$	10.57			
	$^3\Delta_g$	10.58			
	$^3\Sigma_g^+$	10.60			
	$^3\Sigma_g^-$	10.60			
	$^1\Delta_g$	10.62			
	$^1\Sigma_g^+$	10.64			
$4s\sigma_g$	$^3\Pi_g$	10.61			
	$^1\Pi_g$	10.62			
$4p\sigma_u$	$^3\Pi_u$	10.96			
	$^1\Pi_u$	11.10		10.83(R = 1.20)[b]	
$4p\pi_u$	$^1\Sigma_u^-$	10.82			
	$^3\Delta_u$	10.84			
	$^3\Sigma_u^-$	10.85	10.77		
	$^3\Sigma_u^+$	10.86			
	$^1\Delta_u$	10.91	10.78	10.80	
	$^1\Sigma_u^+$	10.93			

[a] The symmetries of these states have been reassigned on the basis of the work by Yamawaki and Ogawa (Ref. 5) and that reported here.

[b] This state appears to contain a large amount of both valence $(3\sigma_u)$ and Rydberg $(3p\sigma_u)$ character.

the same energy as the other $3p\sigma_u$ and $3p\pi_u$ states (e.g., they report the difference between $^3\Sigma_u^-$ and $^3\Pi_u$ to be 0.038 eV). This small splitting between $^3\Sigma_u^-$ and $^3\Pi_u$ is due to the restrictive nature of their basis, which did not have sufficient flexibility to allow the valence $^3\Pi_u$ $(3\sigma_u)$ state to be below the Rydberg $^3\Pi_u$ $(3p\sigma_u)$ state.

A one-electron pseudopotential calculation was carried out on the Rydberg states of O_2 by Betts and McKoy (BM).[24] An exact pseudopotential (as described, for example, by Phillips and Kleinman[25]) has the effect of the Pauli principle built into the potential and leads to correct energies for excited orbitals even though the orbitals are not orthogonal to the core orbitals.[26] The pseudopotential used in the BM calculations was of a very simple semiempirical form. Since they considered only a one-electron problem, they did not distinguish between states of the same orbital configuration (for example, between $^3\Pi_u$ and $^1\Pi_u$ states or between $^3\Sigma_u^-$, $^3\Delta_u$, and $^3\Sigma_u^+$ states). In addition, since this method does not include the lower valence states, they found essentially no splitting between the $^3\Sigma_u^-$ and $^3\Pi_u$ states (whereas a splitting of 0.8 eV is found in the *ab initio* calculations reported here).

Based on IVO calculations[20] on N_2 and CO, the results from the present calculations are expected to agree well with experiment. This expectation is substantiated by comparing the experimental and theoretical ordering and excitation energies summarized in Table III for the $^3\Pi_g$, $^3\Delta_u$, $\beta\,^3\Sigma_u^+$, $^1\Delta_u$, $\alpha\,^1\Sigma_u^+$, and $^1\Pi_u$ Rydberg states. It is seen that not only is the ordering generally correct, but for many states, the experimental excitation energy is close to the predicted value.

IV. RESULTS

A. Location of the $^3\Pi_g$ Rydberg State and the Stability of $O_2^-(^2\Pi_g)$

The structure that appears on top of the Schumann–Runge continuum, in the electron energy-loss spectra such as those shown in Fig. 1, is assumed to be due to the $(3s\sigma_g)\,^3\Pi_g$ Rydberg state $[^3\Pi_g(R)]$, based on comparison with the calculated location and the angular dependence of its differential cross section. The locations and relative intensities for excitation of the vibrational levels of the $^3\Pi_g(R)$ state could be obtained directly from spectra such as those shown in Fig. 1. Table IV contains the measured locations [relative to $X\,^3\Sigma_g^-(v'=0)$], the spacings, and the relative intensities, for the vibrational levels of this state. The analogous quantities known for the $X\,^2\Pi_g$ state[27] of O_2^+, and those for the negative-ion state[11] formed from the $3s\sigma_g$ Rydberg state are also included. The measured spacings for the $^3\Pi_g(R)$ state do not agree particularly well with those for the O_2^+ $(^2\Pi_g)$ state to which it is converging. The relative intensities are in somewhat better agreement except for $v'=0$, which is about 50% larger than might be expected from

TABLE IV. Comparison of the vibrational spacings and relative intensities observed for the $O_2(^3\Pi_g)$, $O_2^+(^2\Pi_g)$ and $O_2^-(^2\Pi_g)$ states.

	$O_2(^3\Pi_g)$			$O_2^+(^2\Pi_g)$ [a]		$O_2^-(^2\Pi_g)$ [b]	
v'	E (eV)	Spacing (eV)	Relative intensity	Spacing (eV)	Relative intensity	Spacing (eV) [c]	Relative intensity
0	8.145 ± 0.020		0.73		0.517		0.73
		0.222		0.232		0.215	
1	8.366 ± 0.020		1.00		1.000		1.00
		0.244		0.228		0.245	
2	8.610 ± 0.020		0.80		0.796		
		0.215		0.224		0.240	
3	8.825 ± 0.020		0.25		0.337		
		...		0.220		0.195	
4	...				0.0818		
		...		0.216			
5	...				0.0114		

[a] Reference 27.

[b] Reference 11(b), Table IV, and text. The structure between 8.0 and 9.0 eV is assumed here to form a vibrational series.

[c] The pairs of numbers given in Table IV of Ref. 11(b) have been averaged to obtain these values.

the Franck–Condon factors for excitation to the $O_2^+(^2\Pi_g)$ state. Transitions to vibrational levels of the $^3\Pi_g(R)$ state greater than $v'=3$ were not observed and are expected to be weak since the potential-energy curve for $O_2\,^3\Pi_g(R)$ should be similar to that of $O_2^+(^2\Pi_g)$. These higher vibrational levels could well be present, and weak as expected, but masked by the steep slope of the high-energy-loss side of the Schumann–Runge continuum (Fig. 1).

Comparison of the spacings and relative intensities given in Table IV leads to two additional observations which help in locating the $^3\Pi_g(R)$ state.

(a) The ratio of the intensity of the $v'=1$ level to that for $v'=0$ is considerably smaller than expected from what is known about the $O_2(X^3\Sigma_g^-) \rightarrow O_2^+(X^2\Pi_g)$ transition, but agrees well with the same ratio determined for the $O_2(X^3\Sigma_g^-) \rightarrow O_2^-(^2\Pi_g)$ transition.[11] That is, both the energy-loss data and the resonance data lead to a $(v'=1)/(v'=0)$ ratio close to 1.36 while the Franck-Condon factors for ionization[27] predict a value of 1.94 for this ratio. The most direct interpretation for this difference is that the internuclear distance for the $^3\Pi_g(R)$ state is somewhat greater than that for the positive state $[R_e(\text{ion})=1.117\ \text{Å}]$ to which it is converging.

(b) The spacing between vibrational levels 1 and 2 in both the $^3\Pi_g(R)$ and $O_2^-(^2\Pi_g)$ states is anomalously large compared to the spacing between $v'=0$ and 1, and to that expected from the corresponding spacings in the $O_2^+(X^2\Pi_g)$ ion state. If all the structures observed by Sanche and Schulz[11(b)] between 8.0 and 9.0 eV [see Fig. 5 and Table IV of Ref. 11(b)] are assumed to be associated with vibrational levels of the same parent state, the averaged vibrational spacings assigned to the $O_2^-(^2\Pi_g)$ state in Table IV are obtained. The vibrational spacings $(E_{v'}-E_{v'-1})$ for the three electronic states given in Table IV are plotted in Fig. 2 as a function of the vibrational quantum number v' for each particular state. The data given for the $O_2^-(^2\Pi_g)$ state are the average of the maximum and the minimum for each feature tabulated by Sanche and Schulz.[11(b)] From Fig. 2 it is evident that both the $O_2(^3\Pi_g)$ and $O_2^-(^2\Pi_g)$ states demonstrate the same large spacing between $v'=1$ and 2; thus this anomaly is real and not an artifact of the present experimental work. One possible explanation for the large spacing observed in the $^3\Pi_g(R)$ state is that it is due to perturbations produced by the crossing, between vibrational levels $v'=1$ and 2, of one or more repulsive-potential-energy curves. There are three lower-lying valence states for which the repulsive inner portions of the potential-energy curves are expected[28,29] to cross the $^3\Pi_g(R)$ state.

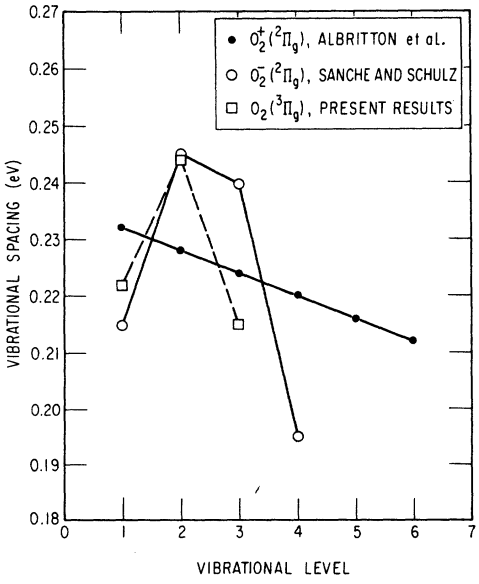

FIG. 2. Vibrational spacings $(E_{v'}-E_{v'-1})$ (eV), as a function of v', for the $(3s\sigma_g)\ ^3\Pi_g$ Rydberg state as determined from the energy-loss spectra. The spacings previously determined for the $O_2^-(^2\Pi_g)$ state by Sanche and Schulz[11(b)] and for the $O_2^+(^2\Pi_g)$ by Albritton *et al.* (Ref. 27) are shown for comparison.

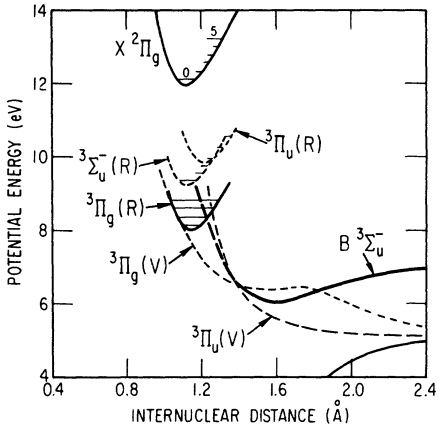

FIG. 3. Potential-energy curves for some of the Rydberg and valence excited states of O_2 obtained by combining the present experimental and theoretical work with the other existing data. The curves for the B state of O_2 and the X state of O_2^+ were taken from Albritton *et al.* (Ref. 27). The curve for the $^3\Pi_g$ Rydberg state has the same shape as for the X state of the ion but has been shifted slightly to larger internuclear distance to allow a larger Franck–Condon factor for excitation of $v'=0$. The repulsive curves for the $^3\Pi_u$ and $^3\Pi_g$ valence states have been placed relative to that for the B state by the calculations of Schaeffer and Harris (Ref. 28) and of Schaeffer and Miller (Ref. 29). The repulsive portion of the $^3\Pi_g$ valence state has been drawn so as to be consistent with the present work and the previous calculations (Ref. 28).

They are the $^3\Pi_g(V)$, $^3\Pi_u(V)$, and $B\,^3\Sigma_u^-(V)$ states. Based on the calculations of Schaeffer and Harris,[28] the $^3\Pi_g(V)$ state is expected to cross the $^3\Pi_g(R)$ state at an internuclear distance equal to or smaller than that associated with its minimum. On the other hand, the $^3\Pi_u(V)$ and $^3\Sigma_u^-(V)$ states, whose potential-energy curves rise more steeply than that for the $^3\Pi_g(V)$ state at these internuclear distances, probably cross the $^3\Pi_g(R)$ state at internuclear distances greater than its minimum. Figure 3 shows the potential-energy curves for the valence and Rydberg states located so as to be consistent with the available experimental and theoretical information on the states in this region. In drawing these curves, heavy solid lines were used for the states which are reasonably well known, as determined by Albritton *et al.*[27] and the present work. The potential-energy curves for the repulsive valence states (dashed curves) were taken from the calculations of Schaefer and Harris,[28] and Schaefer and Miller,[29] but positioned with respect to both the internuclear and energy axes by using the experimentally determined position[27] for the $B\,^3\Sigma_u^-(V)$ state. The shape of the potential-energy curve for the $^3\Pi_g(R)$ state has been drawn to be the same as that for the O_2^+ $(X\,^2\Pi_g)$ state[27] but displaced to larger internuclear distances to be consistent with the greater relative probability of exciting $v'=0$ of the Rydberg state, as discussed above. The potential-energy curve for the $^3\Pi_g(V)$ state cannot yet be located as accurately as for the other states but the combination of the calculations[28] and the analysis of the present data (see below) suggests that the $^3\Pi_g(V)$ state crosses on the left-hand side of the $^3\Pi_g(R)$ state.

The interpretation given above and in Fig. 3 differs somewhat from that given by Sanche and Schulz.[11(b)] They suggest that the $^3\Pi_g(V)$ state crosses the $^3\Pi_g(R)$ state near the potential minimum and, because of an avoided crossing between states of the same symmetry, produces a complete predissociation of the Rydberg state. The negative-ion state associated with the $^3\Pi_g(V)$ state is then required to cross the stable $O_2^-(^2\Pi_g)$ state between $v'=1$ and 2 in order to explain why only two *sharp* levels were observed in their measurements. However, the lowest four vibrational levels of the $^3\Pi_g(R)$ state appear in the energy-loss spectra and therefore this state possesses a well-defined potential well. Based on the information that is available, it is plausible that all the structure observed by Sanche and Schulz[11(b)] between 8 and 9 eV is associated with the $O_2^-(^2\Pi_g)$ state, and that the change in character of their spectra in that energy region is due to perturbations from one or more repulsive valence states.

It is noted that despite the fact that the $^3\Pi_g(V)$ and $^3\Pi_g(R)$ states have the same many-electron symmetry, they should be considered as two independent states in treating dynamic processes in O_2. The reason is as follows: The $^3\Pi_g(V)$ state has the MO configuration $(\ldots 3\sigma_g\,1\pi_u^4\,1\pi_g^3)$ while the $^3\Pi_g(R)$ state has the configuration $(\ldots 3\sigma_g^2\,1\pi_u^4\,1\pi_g\,3s\sigma_g)$. The CI matrix element coupling these states is therefore

$$H_{12}=\langle\,^3\Pi_g(V)|H|^3\Pi_g(R)\rangle=\langle\,3\sigma_g\,|\,K_{1\pi_g}\,|\,3s\sigma_g\rangle\,, \quad (2)$$

where $K_{1\pi_g}$ is the usual exchange operator. The value of this interaction matrix element is 0.015 eV. Thus the spatial width of the crossing region is $\Delta R<0.01$ Å, during which distance the adiabatic wave function changes from $^3\Pi_g(V)$ to $^3\Pi_g(R)$. This ΔR is sufficiently small that the Born–Oppenheimer coupling terms should dominate, leading to two crossing diabatic states, $^3\Pi_g(V)$ and $^3\Pi_g(R)$.

This situation in O_2 appears to be analogous to the Rydberg, non-Rydberg perturbations observed[30] in N_2 in which the homogeneous perturbations between valence and Rydberg states of the same symmetry cause shifting of certain vibrational levels by 200 to 300 cm^{-1}. The values given in Table IV indicate that $v'=1$ and 2 of the O_2 $^3\Pi_g(R)$ state have been shifted by about 210 cm^{-1} (0.026 eV). A similar argument can also be applied to the negative-ion states which result from these $^3\Pi_g$ states and suggests that the $O_2^-(^2\Pi_g)$ state may still be bound above $v'=1$ but more strongly perturbed than the lower levels.

The model that has been implicitly assumed in discussing the electronic states of O_2 involves the usual Born–Oppenheimer separation of electronic and nuclear motion (neglect of nonadiabatic terms), and neglect of the spin-orbit and spin-spin interactions in the total Hamiltonian. Kronig's selection rules,[31] which were derived from consideration of these additional terms, provide a guideline for determining which electronic states will interact and hence those states that could be responsible for the perturbations observed in the vibrational spacing of the $^3\Pi_g(R)$ state. The two selection rules of relevance here are (a) the requirement (rigorous) that the two electronic states have the same inversion symmetry, and (b) the requirement (approximate) that they have the same multiplicity. Of the electronic states presently known to be near the $^3\Pi_g(R)$ state, only the $^{1,3}\Pi_g(V)$ and $^1\Pi_g(R)$ states satisfy selection rule (a). However, because the $^1\Pi_g$ states violate the approximate selection rule (b), they are most likely not responsible for a perturbation in the vibrational spacing of the magnitude observed (0.026 eV = 210 cm^{-1}). The $B\,^3\Sigma_u^-(V)$ and $^3\Pi_u(V)$ states are also excluded on the basis of selection rule (a) above, even

though they probably cross the $^3\Pi_g(R)$ state near $v'=2$. The combination of all the experimental and theoretical information on the $^3\Pi_g(R)$ state leads to the suggestion that the $^3\Pi_g(V)$ state is responsible for the observed perturbation in the vibrational spacing. In addition, the available evidence suggests that the valence state crosses (or grazes) on the left side of the Rydberg state, probably between $v'=1$ and 2.

It is also noted that the four peaks in the energy-loss spectra that are assigned to the $^3\Pi_g(R)$ state are believed to be associated with only one electronic state, rather than a combination of the $^3\Pi_g(R)$ and $^1\Pi_g(R)$ states. This belief is based on the fact that, within experimental error, all four peaks demonstrate the same angular distribution at 45-eV incident-electron energy, for scattering angles from 10° to 70°. If one or more of the observed peaks is due to the $^1\Pi_g(R)$ state, its angular distribution would be expected to differ substantially from that for those associated with the $^3\Pi_g(R)$ state.

The stability, or binding energy, of the loosely bound electron in the $O_2^-(^2\Pi_g)$ state, with respect to the parent $O_2(^3\Pi_g)$ state, can be estimated by combining the results on the negative-ion state with the present results. The lowest vibrational levels for the $O_2^-(^2\Pi_g)$ and $O_2(^3\Pi_g)$ states are at 8.045 and 8.145 eV, respectively. The electron in the $O_2^-(^2\Pi_g)$ state is therefore bound by about 0.10 eV with respect to the parent $O_2(^3\Pi_g)$ state. This is somewhat smaller than that expected based on comparison with other core-excited resonances.[11(b)]

B. Location of the Lowest Dipole-Allowed Rydberg States

The theoretical predictions as to the location of the dipole-allowed Rydberg states, presented in Sec. III, are combined in this section with the energy-loss measurements and other data on these Rydberg states to produce an ordering of the Rydberg states which is consistent with all the information.

The "longest" band[14] at 9.97 eV and "second" band[15] at 10.29 eV are known to represent dipole-allowed transitions because they are strong in both photon absorption[15] and high-energy, small-angle, electron energy-loss spectra.[8] It has not yet been possible to perform a rotational analysis on either of these bands because of their diffuse nature and hence it is not known whether they represent vibrational levels of the same electronic state or levels of different electronic states. Based on the expected quantum defects for excitation to a $^3\Sigma_u^-$ state, Lindholm[32] suggested that the 9.97-eV feature is the third vibrational level of the $^3\Sigma_u^- \leftarrow X^3\Sigma_g^-$ progression beginning at 9.32 eV, and the second (10.29 eV) and third (10.58 eV) bands are vibrational levels four and five, respectively. Although this is a possibility, the measurements of Tanaka[15] on the pressure broadening of these bands indicate that they belong to different electronic states. That is, the longest and third bands pressure broaden primarily toward long wavelengths while the second band pressure broadens more toward short wavelengths. In addition, Tanaka found the third band (10.58 eV) to be much weaker than the other two at low pressure. However, it is noted that the different pressure dependences for these strong bands could be due, in part, to the presence of overlapping bands within the band shape which come from two or more different electronic states having different sensitivity on pressure. The recent work by Yamawaki and Ogawa[5] shows that certain of these strong features are indeed composed of levels from two or more electronic states.

In the calculations reported here, the $^3\Pi_u$ state is predicted to be 0.54 eV *higher* than the $^3\Sigma_u^-$ state, which is calculated as the lowest dipole-allowed state (Table I). In addition, the discussion of the differential cross sections in Sec. IV C indicates that the features in the energy-loss spectra at 9.55 and 9.77 eV are due primarily to vibrational levels of the same electronic state, for which the feature at 9.31 eV may represent $v'=0$. This grouping of these three features was first suggested by Lindholm[32] and appears to be correct based on the theoretical results given above and the experimental data discussed in Sec. IV C. The $(3p\pi_u)\,^3\Sigma_u^-$ state is therefore tentatively placed at $T_{00}=9.31\pm0.02$ eV, athough $v'=0$ could be even lower and buried in the Schumann–Runge continuum.

The $v'=0$ level of the $(3p\sigma_u)\,^3\Pi_u$ state is believed to be located at 9.97 eV, although this interpretation is more difficult to support with experimental results. That is, the relative intensities of the features at 9.97 eV, 10.29 eV, and above in no way resemble that expected for a Rydberg state converging to $O_2^+(^2\Pi_g)$. It is reasonable to assume that the $^3\Pi_u(R)$ state has an internuclear distance fairly close to that for the $O_2(X^3\Sigma_g^-)$ state, which would result in $v'=0$ having by far the greatest intensity. Such a shift in the position of the $^3\Pi_u(R)$ state could be a result of the orthogonality requirement (Sec. III) between the $(3p\sigma_u)$ Rydberg $^3\Pi_u(R)$ state and the lower $(3\sigma_u)$ valence state. As discussed in Sec. III, this orthogonality effect should be stronger at smaller internuclear distances and should result in the Rydberg state having a larger equilibrium distance. This inter-

pretation is consistent with the electron energy-loss and photon absorption measurements.

As a final argument in favor of assigning the $^3\Sigma_u^-$ as the lowest dipole-allowed Rydberg state, a comparison is made between the theoretical oscillator strengths for excitation of the $^3\Sigma_u^-(R)$ and $^3\Pi_u(R)$ states, and the relative intensities observed in photon absorption[15] and small-angle electron scattering.[8] The transition moments, calculated using the dipole-length approximation and the IVO wave functions, for the transitions from the ground state to the lowest $^3\Sigma_u^-(R)$ and $^3\Pi_u(R)$ states, are $0.0513(ea_0)$ and $0.138(ea_0)$, respectively. The corresponding absorption oscillator strengths are calculated (using the theoretical excitation energies) to be 6.2×10^{-4} and 9.4×10^{-3}, respectively. The $^3\Pi_u(R)$ state is therefore predicted to appear at least an order of magnitude stronger than the $^3\Sigma_u^-(R)$ state in photon absorption or small-angle electron scattering. The experimental data[8,15] show that the 9.97-eV longest band is indeed at least 10 times stronger than any of the features at 9.31, 9.55, or 9.77 eV. A more quantitative comparison of the relative strengths of the $^3\Pi_u(R)$ and $^3\Sigma_u^-(R)$ states using experimental data is not possible because it is not yet certain which, if any, of the features appearing at higher excitation energy are vibrational levels of the $^3\Pi_u(R)$ state. For the purposes of identification, the above comparison is sufficient to substantiate the assignment of the $^3\Sigma_u^-$ state as the lowest dipole-allowed Rydberg state.

C. Differential Cross Sections for Several Inelastic Features

Energy-loss spectra such as those shown in Fig. 1, taken as a function of the scattering angle, are useful for obtaining information about the many-electron symmetry of the excited electronic states involved in the various inelastic features.[6] The analysis of such spectra has proved successful in earlier work[9(b)] on the valence excited states of O_2, and will be extended here to the Rydberg states in an effort to determine their symmetry from the experimental data.

1. $^3\Pi_g$ Rydberg State

Figure 4 shows the ratio of the scattering intensity of $v'=1$ of the $^3\Pi_g(R)$ state to those of the 9.97-eV (longest band) and 10.29-eV (second band) features, and the intensity ratio of the latter two, as a function of the scattering angle for an incident electron energy of 45 eV. It is noted that the ratio $(v'=1)/9.97$ eV has a different angular dependence than the ratio $(v'=1)/10.29$ eV. The cause of this difference is shown in the lowest curve in Fig. 4, which shows the intensity ratio of the 9.97- and 10.29-eV features. This ratio has a peculiar shape, which is believed to be due to the presence of other electronic states within the envelopes of the 9.97- and 10.29-eV features. If the overlapping electronic states have sufficiently different angular distributions, an unusual shape in the ratio, such as shown in Fig. 4, can result. The fact that the 9.97- and 10.29-eV features have different differential cross sections for scattering angles greater than about 20° can also be seen from Fig. 5 and 7 of Ref. 9(b).

The recent photon absorption work of Alberti *et al.*[3] and of Ogawa and Yamawaki[33] have placed $v'=2$ of the $\alpha\,^1\Sigma_u^+$ state at 9.92 eV, and $v'=3$ of the $\beta\,^3\Sigma_u^+$ state at 10.05 eV. Both of these levels are close enough to the 9.97-eV feature that they would be unresolved in the present energy-loss experiments and both would be expected to have a differential cross section that differs substantially from that for the dipole-allowed component in the 9.97-eV feature. That is, the Σ^+ states are known[10] to have a vanishing differential cross section as the scattering angle approaches zero degrees for excitation from $X\,^3\Sigma_g^-$, and hence reach their maxima at intermediate scattering

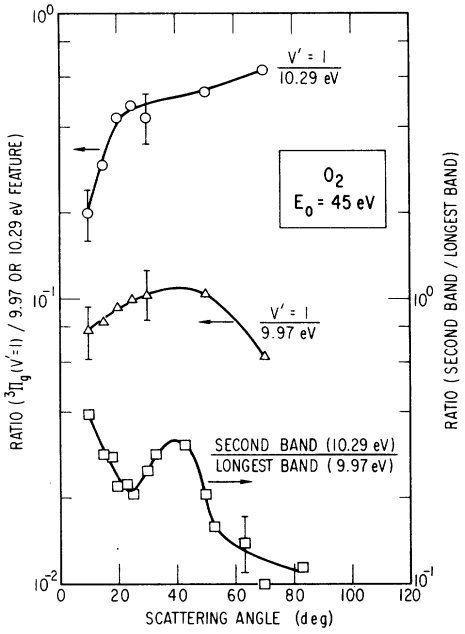

FIG. 4. Ratio of intensity of the $v'=1$ feature from the $^3\Pi_g$ Rydberg state to that of the 9.97 and 10.29-eV bands (left-hand ordinate), as determined from the energy-loss spectra, as a function of the scattering angle, for 45-eV incident electrons. Also shown is the ratio of the intensities for the 10.29- and 9.97-eV features (right-hand ordinate). The error bars shown indicate the typical uncertainty believed to be present in these ratios.

angles. The theoretical results given in Sec. III (Table I) show that the $(3d\sigma_g)\ ^{3,1}\Pi_g$ Rydberg states should have T_{00} values near the 10.29-eV feature. The presence of the additional states within the envelopes of the 9.97- and 10.29-eV features could therefore be responsible for the behavior of the ratio of the 10.29- and 9.97-eV features shown in Fig. 4.

The ratio $^3\Pi_g$ $(v'=1)/10.29$ eV in Fig. 4 (in spite of potential overlap) does display the general behavior expected[34] for the ratio of a symmetry-forbidden to a dipole-allowed transition, for incident energies sufficiently above threshold. That is, the ratio is small at small scattering angles, but increases by about an order of magnitude as the scattering angles increases. This is because, for incident electron energies sufficiently above threshold, the dipole-allowed transitions are more strongly peaked in the forward direction than the symmetry-forbidden transitions. This ratio for a spin-forbidden transition, which has qualitatively the same behavior, can be distinguished from that for a symmetry-forbidden transition, because for the former, the ratio at larger scattering angles is two or three orders of magnitude larger than what it is at the smaller scattering angles.[9(b)] This information, combined with the theoretical results, allows identification of the inelastic features observed on top of the Schumann–Runge continuum as belonging to the $^3\Pi_g$ state.

2. *Features at 9.31, 9.55, and 9.77 eV*

The angular distributions of the other fairly well-defined features appearing in the energy-loss spectra at 45 eV can also be studied. They can be recognized in Fig. 1 as a shoulder on the high-energy-loss side of the Schumann–Runge continuum at about 9.31 ± 0.02 eV, a well-defined peak at 9.55 ± 0.04 eV, and a reasonably well-defined peak at 9.77 ± 0.02 eV. The uncertainty in the energy location for the upper and lower of these three features is due to the fact they are partially overlapped by much stronger components in the spectrum and hence are difficult to locate accurately. As will be discussed below, the maximum of the 9.55-eV feature shifts somewhat depending on the scattering angle, which results in the uncertainty stated for this feature. Some information as to the symmetry of these features can be obtained by plotting the ratios of the intensities of these features to that for the longest band (9.97 eV) and the second band (10.29 eV), and to each other, as a function of the scattering angle. This has been done in Fig. 5 for the 9.55- and 9.77-eV features. The 9.31-eV feature has not been analyzed because of the difficulty in accounting for the steeply rising background from the Schumann–Runge continuum upon which this feature is superposed. The symbols in Fig. 5 represent the data and smooth curves have been drawn through them to aid in identifying their shapes. The first point to be noted from this figure is the striking similarity of the angular dependence for the ratios of the 9.55- and 9.77-eV features to the longest and second bands. Except for differences for scattering angles less than 20°, the ratios of these two features have essentially identical angular dependences. The most probable explanation for this fact is that the 9.55- and 9.77-eV features represent transitions to different vibrational levels of the same electronic state, as has been suggested in Sec. IV C1. Because of the presence of these features in photoabsorption spectra and in small-angle high-energy electron energy-loss spectra, the parent electronic state must be connected to the ground electronic state by dipole selection rules. For the reasons given in Sec. IV C1, the choice most consistent with the available experimental and theoretical information is that this state is the lowest $(3p\pi_u)\ ^3\Sigma_u^-$ Rydberg state.

Although the ratios of the 9.55- and 9.77-eV features to the longest and second bands are remarkably similar, the ratio of the 9.77- to the 9.55-eV feature indicates that there are some small differences at the lower scattering angles.

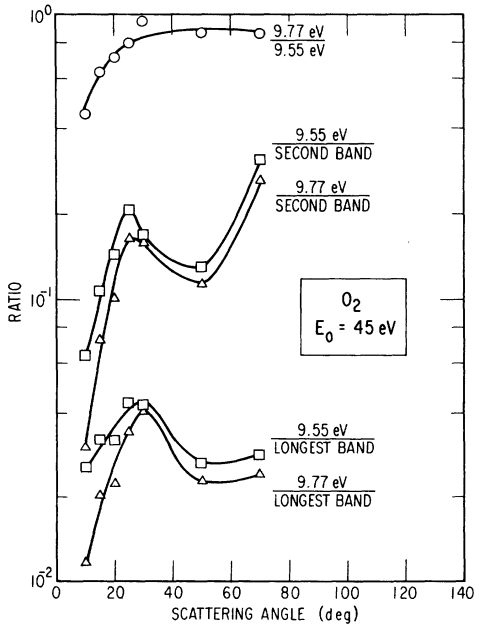

FIG. 5. Ratio of the intensities for the 9.55- and 9.77-eV features to that for the "longest" band (9.97 eV) and "second" band (10.29 eV), as a function of the scattering angle, for 45-eV incident electrons. Also shown is the ratio of the intensities of the 9.77- and 9.55-eV features. See Sec. IV for discussion.

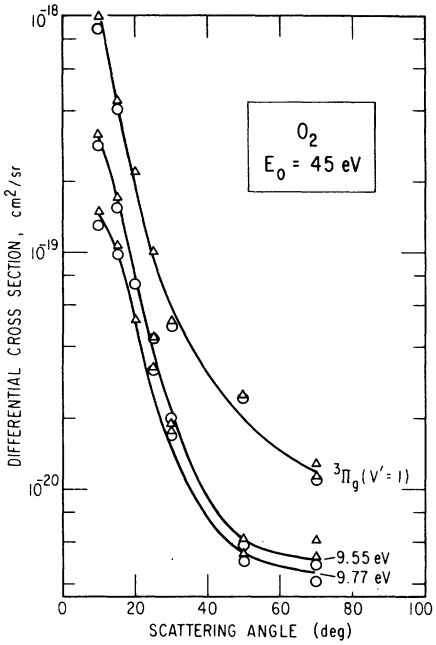

FIG. 6. Normalized differential cross sections for excitation of the $^3\Pi_g$ and the 9.55- and 9.77-eV features, as a function of the scattering angle, for electrons of 45-eV incident energy. The data points were obtained by combining the ratios in Figs. 4 and 5 with the differential cross sections for the 9.97- and 10.29-eV features obtained by Trajmar *et al.* [Ref. 9(b)]. The two data points at certain of the scattering angles means that both the 9.97- and 10.29-eV features were used to obtain an absolute value.

The recent high-resolution photoabsorption work of Alberti *et al.*,[3] Ogawa and Yamawaki,[33] and Yamawaki and Ogawa[5] has resulted in the identification of vibrational levels for the $(n=3)$ $\beta^3\Sigma_u^+$, $^1\Delta_u$, and $^1\Pi_u$ electronic states, which are probably contributing to these electron energy-loss features. Specifically, for the $\beta^3\Sigma_u^+$, $^1\Delta_u$, and $^1\Pi_u$ states $v'=1$, $v'=1$, and $v'=0$, respectively, are calculated[35] to fall at least partially within the envelope of the 9.55-eV feature, and $v'=2$, $v'=2$, and $v'=1$, respectively, fall within the envelope of the 9.77-eV feature. Since the Σ^+ state is not expected to contribute at the small scattering angle owing to the $\Sigma^- \not\rightarrow \Sigma^+$ selection rule,[10] only the $^1\Delta_u$ and $^1\Pi_u$ states can appreciably contribute there. The fact that the 9.77-eV feature increases relative to the 9.55-eV feature can be attributed to the presence of $v'=1$ for the $^1\Pi_u$ state almost precisely under the 9.77-eV feature, while $v'=0$ for this state is about 0.05 eV below the maximum of the 9.55-eV feature. The maximum intensity for the 9.55-eV feature is observed to broaden toward higher energy loss as the scattering angle is increased from smaller to larger scattering angles. The resolution used in these experiments was not sufficient to resolve the structure but this effect most likely can be attributed to contributions from $v'=1$ of the $\beta^3\Sigma_u^+$ state and/or $v'=1$ of the $^1\Delta_u$ progression.

Figure 6 shows the normalized differential cross sections obtained from the energy-loss data for the $^3\Pi_g(R)$ state and the 9.55- and 9.77-eV features. These cross sections were obtained by combining the ratios shown in Figs. 5 and 6 with the normalized differential cross sections for the 9.97- and 10.29-eV features obtained by Trajmar, *et al.*[9(b)] One notes from the figure that the differential cross section for the $^3\Pi_g$ falls off less rapidly with increasing scattering angle than do the 9.55- and 9.77-eV features, for scattering angles greater than about 30°. This is a distinguishing characteristic when comparing symmetry-forbidden and dipole-allowed transitions, as has been discussed earlier.

V. SUMMARY

In this paper *ab initio* quantum-mechanical calculations on the location of the Rydberg states of O_2, and electron energy-loss data which show some of these states, are reported. These results are then correlated with electron transmission and photon absorption measurements to identify and locate the first $(n=3)$ members of the Rydberg series $(ns\sigma_g)$ $^3\Pi_g$, $(np\pi_u)$ $^3\Sigma_u^-$, and $(np\sigma_u)$ $^3\Pi_u$, which converge to the O_2^+ $(^2\Pi_g)$ state. These lowest members are located at $T_{00}=8.145\pm0.020$, 9.31 (or possibly 9.05), and 9.97 eV, respectively. The combination of the information indicates that the $(3s\sigma_g)$ $^3\Pi_g$ state is crossed on the left near $v'=2$ by the $^3\Pi_g(V)$ state and has an equilibrium internuclear distance greater than that for the O_2^+ $(^2\Pi_g)$ state. Comparison of the location for the O_2^- $(^2\Pi_g)$ state with the present results for the $^3\Pi_g(R)$ state results in a binding energy of 0.10 eV for the $^3\Pi_g(R)$ state plus an electron.

The $^3\Sigma_u^-(R)$ state is determined to be below the $^3\Pi_u(R)$ state as a result of the good agreement between the calculated and measured locations and relative intensities for these two states. The $^3\Pi_u(V)$ state is believed to have a strong effect on the $^3\Pi_u(R)$ state and produce an equilibrium internuclear distance for the $^3\Pi_u(R)$ state which is closer to that for the O_2 $(X^3\Sigma_g^-)$ state than to the O_2^+ $(^2\Pi_g)$ to which it is converging.

Normalized differential cross sections for excitation of the Rydberg $^3\Pi_g$, $^3\Sigma_u^-$, and $^3\Pi_u$ states have been obtained, for incident electrons of 45-eV energy.

ACKNOWLEDGMENTS

The authors would like to thank M. Ogawa and K. R. Yamawaki of USC and L. Sanche and G. L.

Schulz of Yale for providing the results of their work prior to publication. The cooperation of D. Albritton of NBS–Boulder in providing the spectroscopic data of O_2 and O_2^+ prior to publication was greatly appreciated. Stimulating conversations with Thom Dunning of Caltech, Y. Tanaka of AFCRL, and M. Ogawa of USC were helpful in formulating the interpretation presented in this paper. The excellent computational help of N. A. Fiamengo of Aerospace in the analysis of the experimental data is gratefully acknowledged.

---

†Work partially supported by USAF SAMSO Contract F04701-72-C-0172 to The Aerospace Corporation; the Caltech President's Fund (PF-013), Contribution No. 4670; and NASA Contract No. NAS7-100 to JPL.

*NDEA Fellow; present address: Department of Chemistry, University of California, Berkeley, California 94720.

‡Partially supported by Grant (GP-15423) from the NSF.

[1]A thorough review of the work that has been done on O_2 is contained in the recent work by Paul H. Krupenie, J. Phys. Chem. Ref. Data 1, 423 (1972).

[2]Y. Tanaka, A. S. Jursa, F. J. LeBlanc, and E. C. Y. Inn, Planet. Space Sci. 1, 7 (1959).

[3]F. Alberti, R. A. Ashby, and A. E. Douglas, Can. J. Phys. 46, 337 (1968).

[4]M. Ogawa, J. Chem. Phys. 53, 3754 (1970).

[5]K. R. Yamawaki and M. Ogawa (unpublished).

[6]S. Trajmar, J. K. Rice, and A. Kuppermann, Adv. Chem. Phys. 18, 15 (1970).

[7]See E. N. Lassettre, Can. J. Chem. 47, 1934 (1969), and references therein.

[8]J. Geiger and B. Schroeder, J. Chem. Phys. 49, 740 (1968).

[9](a) S. Trajmar, D. C. Cartwright, and W. Williams, Phys. Rev. A 4, 1482 (1971); (b) S. Trajmar, W. Williams, and A. Kuppermann, J. Chem. Phys. 56, 3759 (1972).

[10]D. C. Cartwright, S. Trajmar, W. Williams, and D. L. Huestis, Phys. Rev. Lett. 27, 704 (1971); W. A. Goddard III, D. L. Huestis, D. C. Cartwright, and S. Trajmar, Chem. Phys. Lett. 11, 329 (1971).

[11](a) L. Sanche and G. J. Schulz, Phys. Rev. Lett. 26, 943 (1971); (b) L. Sanche and G. J. Schulz, Phys. Rev. A 6, 69 (1972).

[12]A preliminary version of the results in this paper was presented at the 27th Symposium on Molecular Structure and Spectroscopy, Columbus, Ohio, 1972 (unpublished).

[13]S. Trajmar, D. G. Truhlar, and J. K. Rice, J. Chem. Phys. 52, 4502 (1970).

[14]W. C. Price and G. Collins, Phys. Rev. 48, 714 (1935).

[15]Y. Tanaka, J. Chem. Phys. 20, 1728 (1952).

[16]W. J. Hunt, T. H. Dunning, and W. A. Goddard, Chem. Phys. Lett. 3, 606 (1969); W. A. Goddard, T. H. Dunning, and W. J. Hunt, Chem. Phys. Lett. 4, 231 (1969); W. J. Hunt, W. A. Goddard, and T. H. Dunning, Chem. Phys. Lett. 6, 147 (1970).

[17]W. J. Hunt and W. A. Goddard III, Chem. Phys. Lett. 6, 414 (1969).

[18]H. Lefebvre-Brion and G. M. Moser, J. Chem. Phys. 43, 1394 (1965).

[19]T. H. Dunning, Jr., J. Chem. Phys. 53, 2823 (1970).

[20]W. J. Hunt, thesis (The California Institute of Technology, 1971) (unpublished).

[21]W. J. Hunt, P. J. Hay, W. A. Goddard, J. Chem. Phys. 57, 738 (1972).

[22]The version used is basically that due to H. Basch.

[23]J. LeClercq, Ann. Astrophys. 30, 93 (1967).

[24]T. Betts and V. McKoy, J. Chem. Phys. 54, 113 (1971).

[25]J. C. Phillips and L. K. Kleinman, Phys. Rev. 116, 287 (1959).

[26]C. F. Melius, W. A. Goddard, and L. R. Kahn, J. Chem. Phys. 56, 3342 (1972).

[27]D. L. Albritton, A. L. Schmeltekopf, and R. N. Zare, *Diatomic Intensity Factors* (Harper and Row, New York, to be published).

[28]H. F. Schaefer III and F. E. Harris, J. Chem. Phys. 48, 4946 (1968).

[29]H. F. Schaefer III and W. H. Miller, J. Chem. Phys. 55, 4107 (1971).

[30]K. Dressler, Can. J. Phys. 47, 547 (1969); P. K. Carroll and C. P. Collins, Can. J. Phys. 47, 563 (1969).

[31]G. Herzberg, *Spectra of Diatomic Molecules* (van Nostrand, Princeton, N. J., 1957), p. 285; I. Kovacs, *Rotational Structure in the Spectra of Diatomic Molecules* (American Elsevier, New York, 1969), p. 199.

[32]E. Lindholm, Ark. Phys. 40, 117 (1969).

[33]M. Ogawa and K. R. Yamawaki, Can. J. Phys. 47, 1805 (1969).

[34]This can be seen in the case of He ($2\,^1S$) excitation in Fig. 3 of J. K. Rice, D. G. Truhlar, D. C. Cartwright, and S. Trajmar, Phys. Rev. A 5, 767 (1972), for energies of the order of 50 eV above threshold.

[35]For those lower vibrational levels of these states which have not yet been located experimentally, the locations of the levels were extrapolated from the known locations of the higher levels by using the vibrational spacings in the O_2^+ ($^2\Pi_g$) state.